RAA 2016 Vol. **16** No. **8**, 119 (8pp) doi: 10.1088/1674–4527/16/8/119
http://www.raa-journal.org *http://iopscience.iop.org/raa*

***R**esearch in*
***A**stronomy and*
***A**strophysics*

Subreflector model depending on elevation for the Tianma 65 m Radio Telescope

Zheng-Xiong Sun[1], Jin-Qing Wang[1] and Lan Chen[2]

[1] Shanghai Astronomical Observatory, Chinese Academy of Sciences, Shanghai 200030, China; *zxsun@shao.ac.cn*
[2] Shanghai Institute of Technology, Shanghai 201400, China

Received 2015 August 25; accepted 2016 March 2

Abstract A subreflector adjustment system for the Tianma 65 m radio telescope, administered by Shanghai Astronomical Observatory, has been installed to compensate for gravitational deformation of the main reflector and the structure supporting the subreflector. The position and attitude of the subreflector are variable in order to improve the efficiency at different elevations. The subreflector model has the goal of improving the antenna's performance. A new fitting formulation which is different from the traditional formulation is proposed to reduce the fitting error in the Y direction. The only difference in the subreflector models of the 65 m radio telescope is the bias of a constant term in the Z direction. We have investigated the effect of movements of the subreflector on the pointing of the antenna. The results of these performance measurements made by moving the antenna in elevation show that the subreflector model can effectively improve the efficiency of the 65 m radio telescope at each elevation. An antenna efficiency of about 60% at the Ku band is reached in the whole angular range of elevation.

Key words: telescopes — methods: observational — methods: data analysis

1 INTRODUCTION

The Tianma 65 m (TM65 m) radio telescope is a large telescope with a Cassegrain configuration composed of a 65 m diameter parabolic primary reflector and a 6.5 m diameter secondary reflector. The weight of the antenna is about 2740 t and the maximum operating frequency is 43 GHz. The antenna is sensitive to eight bands (L, S, C, X, Ku, K, Ka, Q) covering almost 70% of the frequency range below 50 GHz. In order to maintain the optimum parabolic shape of the main reflector, the block panel of the main reflector has a wide adjustment range of $\pm$15 mm and with a precision of around 15 μm (Wang et al. 2008). In the process of observation, the structures supporting the subreflector, the back frame of the main reflector and the main reflector have different degrees of deformation (Dou & Yao 2012). Furthermore, the subreflector has shifts induced by gravity and by thermal deformations that produce tilts with respect to its ideal optical alignment. Six linear electro-mechanical actuators that are part of a Stewart mechanism allow the subreflector to move over the main reflector with a maximum extension range that can compensate for gravitational deformation of the main reflector and the supporting structure (Greve et al. 1994).

The aim of this paper is to increase the antenna efficiency as high as possible by constructing a model to determine changes in the position and attitude of the subreflector with elevation. Moreover, some gravitational deformation of the main reflector cannot be fully compensated by adjusting the main reflector. A wider range for compensating the optical path can be achieved by adjusting the subreflector. In order to fulfill the requirement for the TM65 m of operating at high frequencies, adjusting the position and attitude of the subreflector is a key factor to compensate for optical misalignments by utilizing actuators mounted on the subreflector. We have also investigated the effect of movements of the subreflector in the pointing of the antenna. In this study, we have measured the pointing error by scanning the antenna with changes in elevation. The performances at the Ku band are good and successfully meet the requirements for precision of TM65 m. In the model, a new fitting formulation, which is different from the one in low-frequency bands of TM65 m, is proposed to fit the data and it can greatly reduce the fitting errors.

One practical difference between optical telescopes and the TM65 m is that optical telescopes have detectors that can form images instantaneously, but the TM65 m only has one beam, or multiple beams separated by several beamwidths. Thus, astronomical calibration of the TM65 m involves scans whose outputs are one-dimensional, roughly Gaussian, functions of azimuth or elevation, subreflector offsets, etc. The parameters of interest are normally the centroid position and peak of the observed

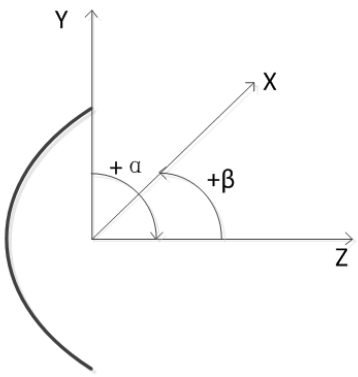

Fig. 1 Definition of coordinates used by the subreflector.

Gaussian which can be determined by least squares fitting (Yu et al. 2015).

2 THE POSITION AND ATTITUDE OF THE SUBREFLECTOR

The subreflector support system has a hexapod design. The six linear electro-mechanical actuators allow the subreflector to move in space over the main reflector: lateral displacements x and y, axial movement along the z axis, and tilts around the x and y axis. The subreflector shifts with the following specifications: a displacement range of $\pm$100 mm in x, y, z directions with an accuracy of $\pm$0.05 mm; an angular range of –2°$\sim$+8° around the X direction with an accuracy of 10″; and an angular range of $\pm$2° around the Y direction with an accuracy of 10″. In operation, the software interface allows control of five degrees freedom. The six rod displacement values of the Stewart mechanism are driven by the control computer for the subreflector, then the actuators that are part of the Stewart mechanism drive the six ball screws to the target locations. The coordinate system used by the subreflector of the TM65 m radio telescope follows the right hand rule as shown in Figure 1. When the antenna is placed horizontally, the X-axis is parallel to the elevation axis of the antenna; the Y-axis is parallel to the elevation gear plane (when the antenna is horizontal, it is the direction of gravity); the Z direction is the outward direction along the focus; α is the rotation around the X-axis; and β is the rotation around the Y-axis.

The displacement of the Z-axis, the Y-axis as well as α will exhibit relatively large variations when the antenna is moving in its elevation range. Figure 2 shows the change in the position and attitude of subreflector with respect to the main reflector when the antenna moves in elevation from 90° to 40°. The behavior of the subreflector displays the following characteristics: the location of the center decreases by Δy; the focus shortens by Δz; the tilt angle varies by $\Delta\alpha$.

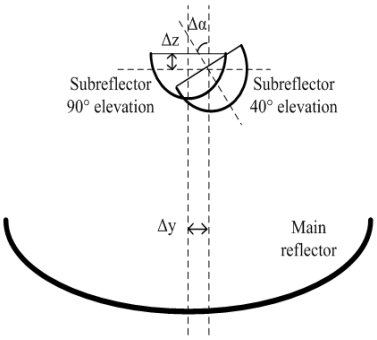

Fig. 2 Change in the subreflector position relative to the main surface caused by different elevations.

3 RADIAL AND AXIAL DISPLACEMENTS OF THE SUBREFLECTOR

Lateral displacements of the subreflector will cause asymmetries in the beam, a small decrease in the antenna gain and obvious pointing offsets which depend on the geometry of the antenna. We targeted some observations around 3C 286 with elevation and azimuth scans. The scan rate should be fairly high to save time and minimize baseline drifts.

Figures 3 and 4 show horizontal and vertical cuts of the beam when targeting 3C 286 around an elevation of 55°. The radial displacement that causes asymmetry and pointing offsets can be easily seen.

Figure 5 shows axial cuts of the beam when targeting 3C 286 around an elevation of 55°. The axial displacement of the subreflector causes gain to dramatically decrease.

4 THE MODEL OF SUBREFLECTOR

An axial displacement of the focus is along the Z-axis, which ideally should coincide with the paraboloid and hyperboloid axis. It causes a change in the intensity of the detected signal and a widening of the beam width of the antenna. Therefore, the best axial focus is determined by measuring the intensity at different focal positions and at different elevations. Table 1 summarizes the initial values of the position and attitude of the subreflector.

Axial focus determination is achieved by calculating the peak of the Gaussian determined by least squares fitting to the signal which is detected at different displacements in the Z direction. Then the maximum of the parabola is obtained by fitting the previously solved peak values. Each data set consists of five or six different positions of the focus, with a total displacement of two wavelengths.

Figure 6 depicts the intensity values of the detected signal at an elevation of 55° for five different Z values of the subreflector. A parabola can be fitted to the five points in each series. The maximum of the parabola is determined to be –2 mm.

The final result is visible in Figure 7 where we present the best Z position from 13° to 80°. The more negative the value, the smaller the distance between the main reflec-

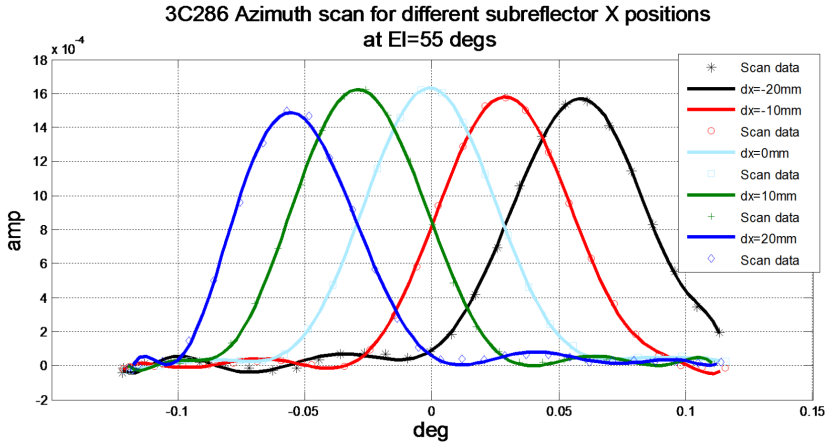

Fig. 3 Horizontal cut of the antenna beam at 13.5 GHz with different X positions of the subreflector. The cut was obtained by making azimuth drifts around an elevation of 55° when targeting 3C 286. The change in pointing due to the displacement of the subreflector was not corrected. Hence, the main lobe was located at a different position.

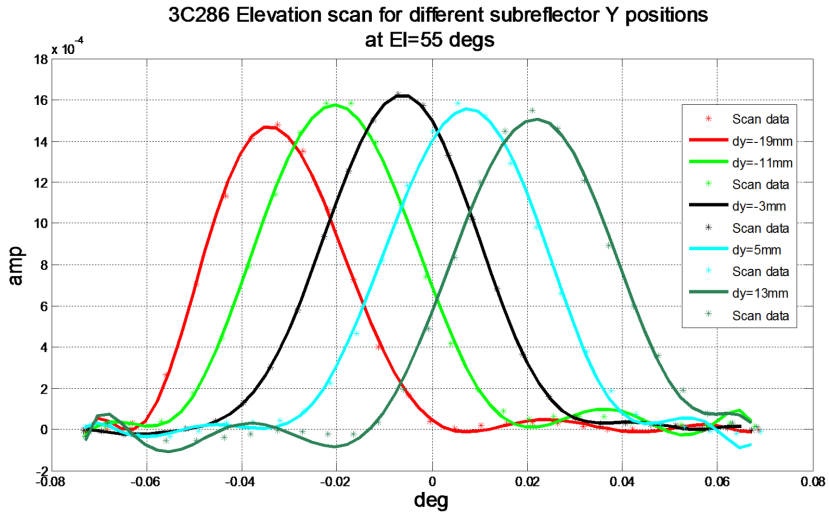

Fig. 4 Vertical cut of the antenna beam at 13.5 GHz with different Y positions of the subreflector. The cut was obtained by measuring elevation drifts around an elevation of 55° when targeting 3C 286. The change in pointing due to the displacement of the subreflector was not corrected. Hence, the main lobe was located at a different position.

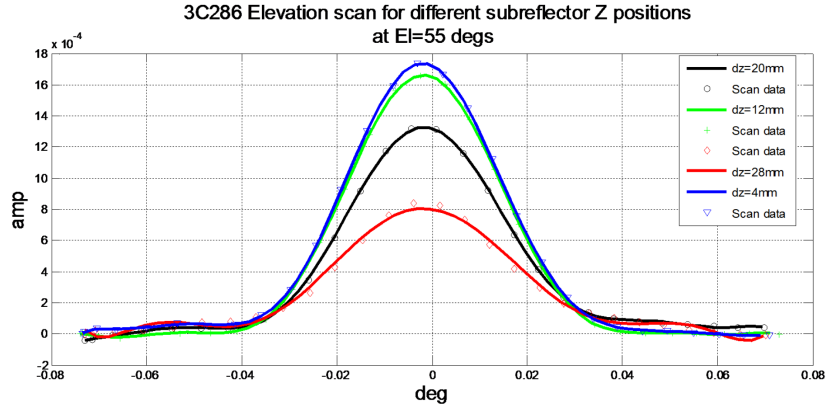

Fig. 5 Axial cut of the antenna beam at 13.5 GHz with different Z positions of the subreflector. The cut was obtained by measuring elevation drifts around an elevation of 55° when targeting 3C 286. In this case, the axial displacement of the subreflector did not influence the pointing. Hence, the main lobe was located at the central position.

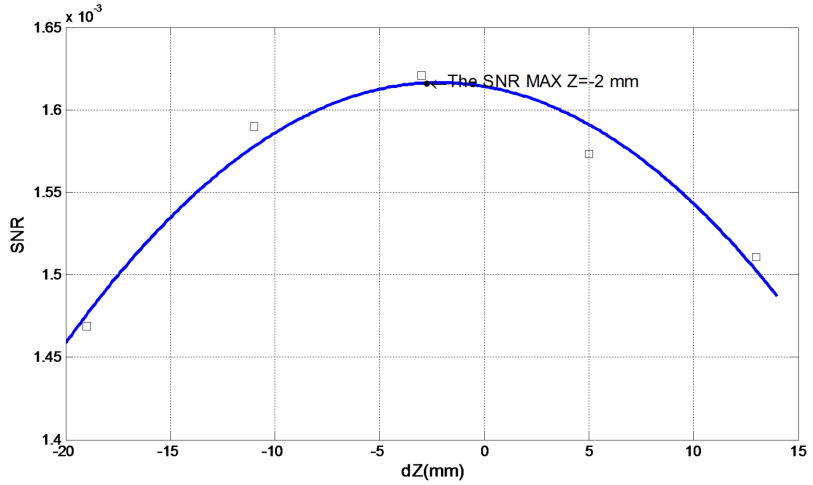

Fig. 6 Best Z position fitting @EL=55°.

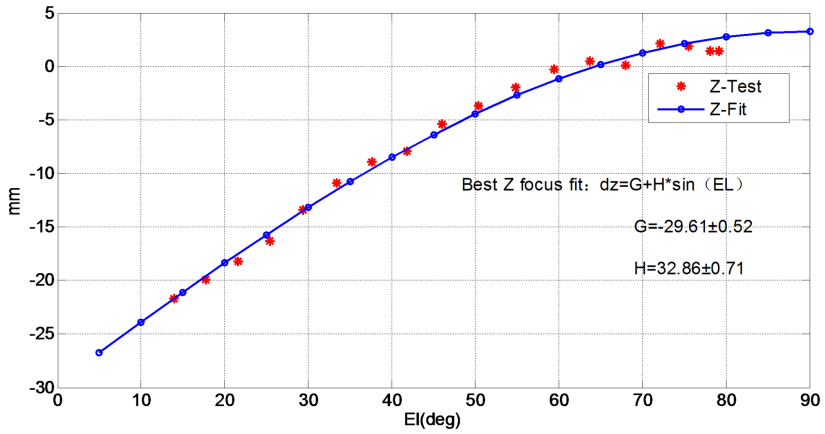

Fig. 7 Fit of the Z focus versus elevation.

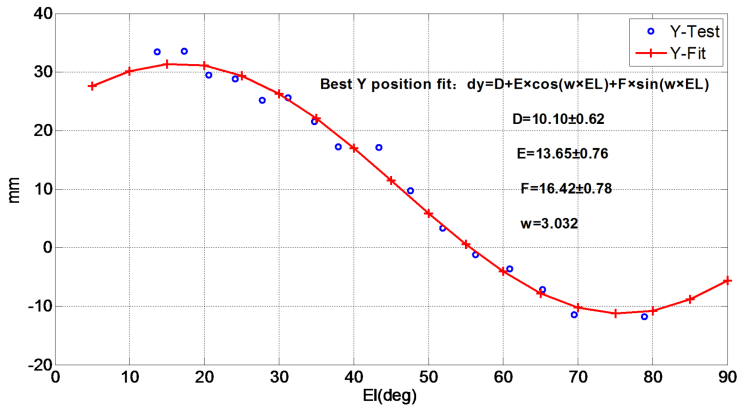

Fig. 8 Best subreflector position along Y versus elevation. This position was fit after the Z focus was already determined.

Table 1 Initial Position of the Subreflector

X (mm)	Y (mm)	Z (mm)	α (°)	β (°)
2.434	13.553	11.93	0.065	−0.072

tor and the subreflector. The total displacement of the focus from 5° to 90° according to this measurement is about 30 mm, which is probably due to the gravitational pull and the design of the antenna, both of which affect its shape and the focus position.

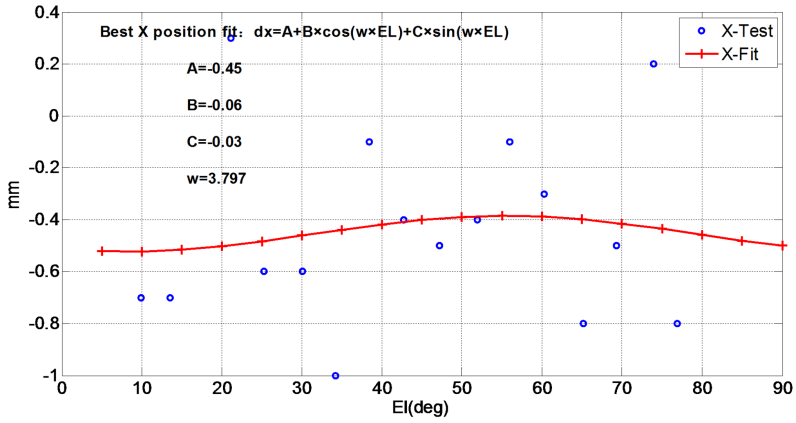

Fig. 9 Best subreflector position along X versus elevation. This position was fit after the Z focus was already determined.

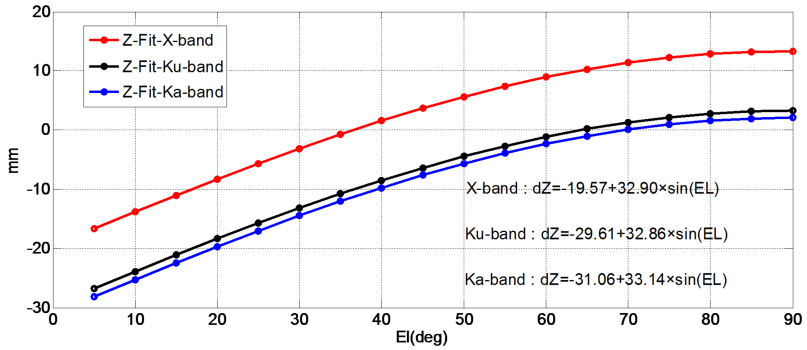

Fig. 10 Subreflector position model in the Z direction.

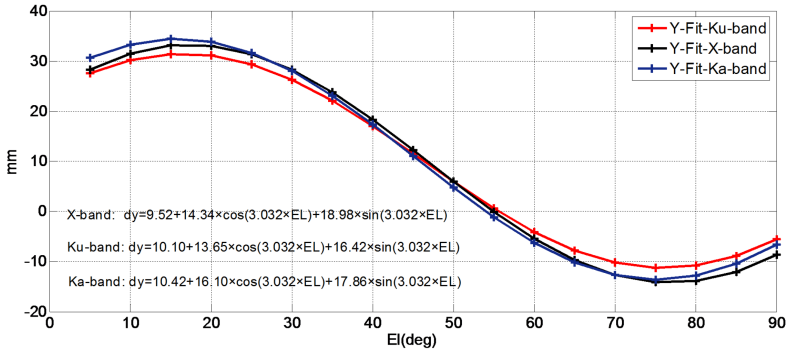

Fig. 11 Subreflector position model in the Y direction.

We investigated the behavior of the subreflector along the Y axis and X axis by making scans on quasar 3C 286 and compiling the best Y position values with different elevations. Equation (1) is the polynomial used to calculate the model of the 40 m radio telescope at the Yebes Observatory located in Spain.

$$dy = a1 + a2 \times \cos(\mathrm{EL}). \qquad (1)$$

Using Equation (1) for the fitting model of TM65 m in the Y direction, the rms is 3.419 and the error fitting coefficients respectively are 2.72 and 3.71. Apparently, the error is too large to satisfy the requirement for precision. Equation (2) is the polynomial used to build the model of Green Bank Telescope.

$$dy = b1 + b2 \times \cos(\mathrm{EL}) + b3 \times \sin(\mathrm{EL}). \qquad (2)$$

Using Equation (2) for the fitting model of TM65 m in the Y direction, the rms is 2.443 and the error fitting coefficients respectively are 2.56, 2.64 and 2.62. The errors are smaller than the ones from using Equation (1). However, the results do not meet the requirement. In order to find a

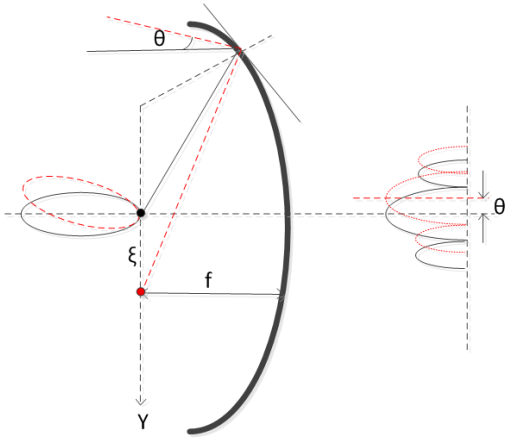

Fig. 12 Pointing deviation caused by focus offset in the Y direction.

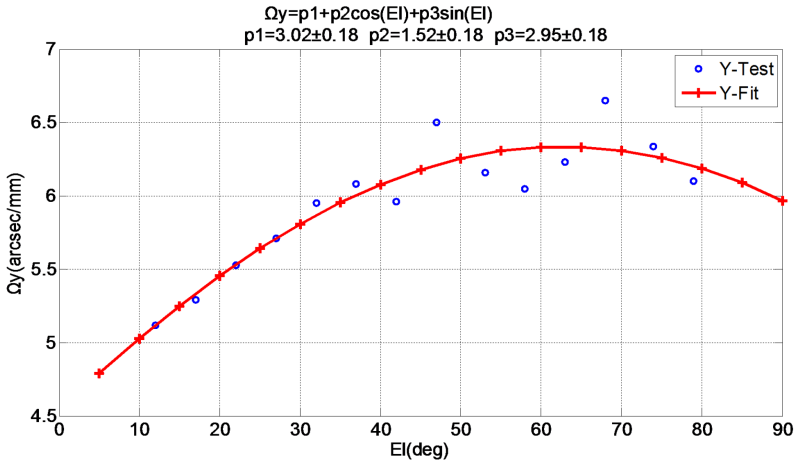

Fig. 13 Ω_Y model–Unit displacement in the Y direction that results in deflection of the elevation point.

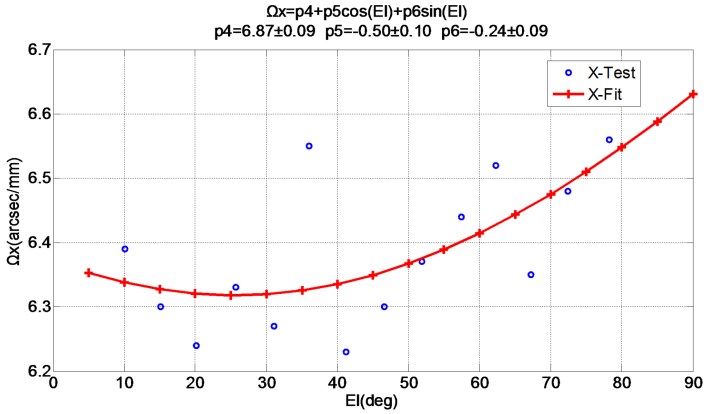

Fig. 14 Ω_X model–Unit displacement in the X direction that results in azimuth point deflection.

better polynomial, we considered improvement on the basis of Equation (2). A Fourier polynomial can nicely fit the data that we observed. Equation (3) is the ultimate polynomial used to build the model of TM65 m in the Y direction. The rms is 1.713 and the error fitting coefficients respectively are 0.62, 0.76 and 0.78. Obviously, the fitting error decreases a lot, which greatly improves the accuracy of the model in the Y direction. Therefore, Equation (3) is also used to build the model in the X direction. The results are shown in Figures 8 and 9.

$$dy = c1 + c2 \times \cos(w \times \mathrm{EL}) + c3 \times \sin(w \times \mathrm{EL}). \quad (3)$$

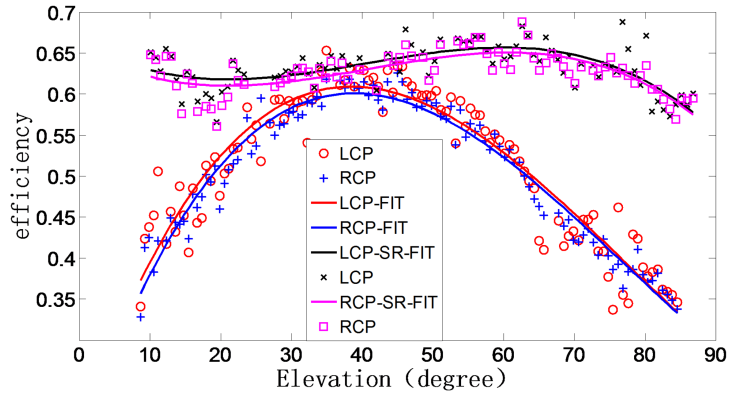

Fig. 15 The efficiency test of Ku-band for left and right circular polarization channels @3C 286,13.5 GHz and 20 MHz bandwidth.

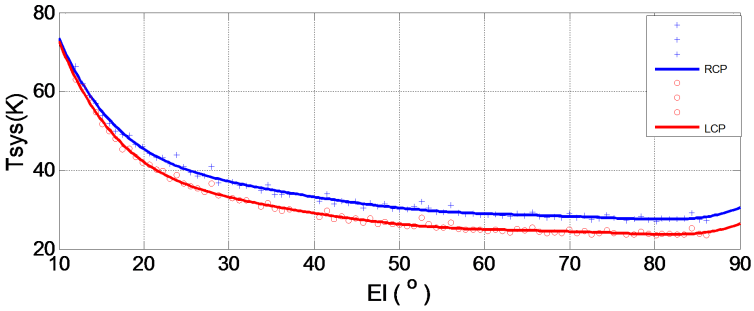

Fig. 16 System temperature @3C 286, 13.5 GHz and 20 MHz bandwidth.

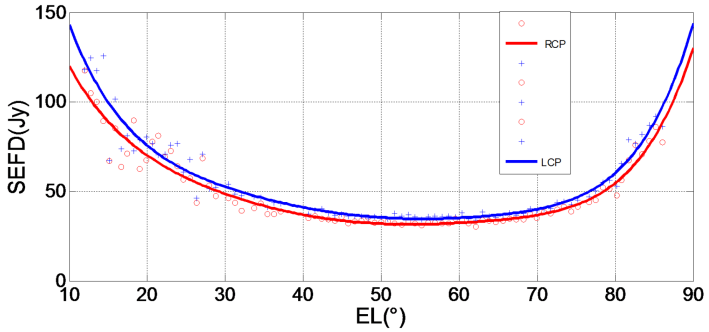

Fig. 17 SEFD measurement @3C 286, 13.5 GHz and 20 MHz bandwidth.

The Y position of the subreflector varies from 33 mm at an elevation of 14° to –12 mm at an elevation of 80°. This means that the subreflector apparently "falls" along the Y axis when the antenna is tilted towards the horizon. The most probable explanation is that the supporting legs of the hexapod suffer from gravitational flexure (Wang et al. 2015a). However, the subreflector shows an approximately constant shift in the X axis, which does not depend on elevation. This is because the antenna is symmetrical along the elevation axis.

We have fitted a model to the data. Our best fit is (Sun et al. 2016):

$$\begin{aligned} dX &= -0.45 - 0.06 \times \cos(3.797 \times \mathrm{el}) \\ &\quad -0.03 \times \sin(3.797 \times \mathrm{el})\,, \qquad (4) \\ dY &= 10.10 + 13.65 \times \cos(3.023 \times \mathrm{el}) \\ &\quad +16.42 \times \sin(3.023 \times \mathrm{el})\,, \qquad (5) \\ dZ &= -29.61 + 32.86 \times \sin(\mathrm{el})\,, \qquad (6) \end{aligned}$$

where el is the elevation in the unit of radian.

Figures 10 and 11 respectively depict the comparison of the subreflector model in the Z and Y directions at the X, Ku, Ka bands. As we can see, the curves representing the Y-model show little difference and the Z-model has a bias that is a constant term. This is because the phase centers of different receivers are not the same along the Z-axis.

5 POINTING EFFECTS

We have also investigated the effect of movements of the subreflector in the pointing of the antenna. Displacements of the subreflector in X and Y and tilts around X and Y cause a change in the pointing. The changes in pointing are obtained by calculating the model of the subreflector for each observation. Consequently, the pointing errors due to radial displacements of the subreflector need to be compensated by Equations (7) and (8). Ω_Y indicates the elevation pointing deviation value due to unit displacement in the Y direction and Ω_X indicates the azimuth pointing deviation value due to the unit displacement in the X direction. Surprisingly, we have also noticed that the two coefficients are not approximately constant values but rather are related to the elevation angle of the antenna.

Figure 12 shows that the offset direction of the subreflector is opposite to the direction of the pointing deviation induced by movements of the subreflector. Here the dotted line denotes the pointing deflection of the pattern caused by shifting of the focus (Wang et al. 2014). Figures 13 and 14 respectively show the measured values of Ω_Y and Ω_X related to the elevation angle of the antenna.

$$\Delta\mathrm{EL} = \Omega_Y \times Y, \tag{7}$$

$$\Delta\mathrm{AZ} = \Omega_X \times X. \tag{8}$$

6 EFFICIENCY, SYSTEM TEMPERATURE AND SEFD

We have measured the efficiency of the antenna in both the left and right circular polarization (LCP and RCP respectively) channels by using the radio source 3C 286 at the Ku band. We made two series of measurements, applying and not applying the model during the night, by moving the antenna in elevation from 10° to 85° with a 1° step and acquiring data at each elevation position. Before measuring the efficiency in each case, the five points method was used to revise the pointing, thus correcting the residual error of the pointing model in the entire zone. The test result indicates that the subreflector model can effectively improve the efficiency of the TM65 m radio telescope at both high and low elevations.

Figure 15 shows the antenna efficiency versus elevation, where the label LCP-FIT represents the left circular efficiency test while not applying the model; RCP-FIT represents the right circular efficiency test while not applying the model; LCP-SR-FIT represents the left circular efficiency test while applying the model; and RCP-SR-FIT represents the right circular efficiency test while applying the model.

Figure 16 shows measurements of the system temperature at the Ku band. System temperature includes atmosphere temperature, antenna temperature, receiver temperature and ground leakage. Although the receiver temperature does not vary along with the change in antenna elevation, the atmosphere temperature at the antenna is related to elevation (Wang et al. 2015b). For the radio telescopes we can measure the sensitivity of the system by System Equivalent Flux Density (SEFD). It is defined as the ratio of the system temperature to the Degree Per Flux Unit (DPFU). The smaller the value, the higher the sensitivity of the antenna. Figure 17 shows the antenna sensitivity at the Ku band.

Acknowledgements This work is supported by the National Natural Science Foundation of China (No. U1531135). We are very grateful to the anonymous referee for his/her helpful suggestions for improving our work.

References

Dou, Y. C., & Yao, J. T. 2012, Robot, 34, 399

Greve, A., Morris, D., Johansson, L., Whyborn, N., & Gluiber, A. 1994, in Microwaves, Antennas and Propagation, IEE Proceedings, 141, 23

Sun, Z.-X., Wang, J. Q., W., & Chen, L. 2015, in 2015 Asia-Pacific Microwave Conference (APMC), 1, IEEE, 1

Wang, J. Q., Zhao, R. B., Yu, L. F., et al. 2015a, Acta Astronomica Sinica, 56, 278

Wang, J. Q., Yu, L. F., Zhao, R. B., et al. 2015b, Acta Astronomica Sinica, 56, 63

Wang, J., Yu, L., Zhao, R., et al. 2014, Scientia Sinica Physica, Mechanica & Astronomica, 44, 1232

Wang, W., Duan, B.-Y., & Ma, B.-Y. 2008, Acta Electronica Sinica, 6, 014

Yu, L. F., Wang, J. Q., Zhao, R. B., et al. 2015, Acta Astronomica Sinica, 56, 165